

RSC Advances



This is an *Accepted Manuscript*, which has been through the Royal Society of Chemistry peer review process and has been accepted for publication.

Accepted Manuscripts are published online shortly after acceptance, before technical editing, formatting and proof reading. Using this free service, authors can make their results available to the community, in citable form, before we publish the edited article. This *Accepted Manuscript* will be replaced by the edited, formatted and paginated article as soon as this is available.

You can find more information about *Accepted Manuscripts* in the [Information for Authors](#).

Please note that technical editing may introduce minor changes to the text and/or graphics, which may alter content. The journal's standard [Terms & Conditions](#) and the [Ethical guidelines](#) still apply. In no event shall the Royal Society of Chemistry be held responsible for any errors or omissions in this *Accepted Manuscript* or any consequences arising from the use of any information it contains.

Single step synthesis of 'silver-polymer hybrid material' and its catalytic application

Meenakshi Choudhary, Samarjeet Siwal and Kaushik Mallick*

Department of Chemistry, University of Johannesburg, P.O. Box: 524, Auckland Park 2006, South Africa.

* Corresponding Author

E-mail: kaushikm@uj.ac.za

Abstract: Conjugated polymer stabilized silver nanoparticles has been synthesized using an *in-situ* polymerization and composite formation (IPCF) method.¹ The optical property of the composite material was studied employing FTIR, UV-visible and fluorescence spectroscopy techniques. Electron microscopic image showed silver nanoparticles within the size range of 7-12 nm are uniformly dispersed within the polymer matrix. The as-prepared metal-polymer nanocomposites exhibited excellent catalytic activity for the reduction of 4-nitrophenol ion. The polymer based composite material also possesses the electro-sensing activity towards the enzyme-free detection of hydrogen peroxide in a very efficient and sensitive pathway.

Introduction:

Nanocomposites are a special class of high performance material derived from the successful combination of the characteristics of the original constituents into a single material using some suitable techniques. By incorporating the inorganic nanomaterials in to the organic polymer, the properties of polymers, such as, optical, electrical and magnetic, either has been changed or improved.¹⁻³ The synthesis of polymer based nanocomposites is an integral aspect of polymer nanotechnology and the materials scientists handle such nanocomposites to extract the unique physical properties and wide application potential in diverse areas.

For the development of smart polymer nanocomposite matrices, a hybrid system consisting of maghemite (Fe₂O₃)-gold 'core-shell' nanoparticles and polyaniline composite has been reported for the magneto-switchable bio-electrocatalytic oxidation of glucose.⁴ Polyaniline is a popular conducting polymer due to its simple synthesis process, good electrical conductivity, environmental stability and doping dependent variable redox properties.⁵ Carbon based nanostructured materials are also considered as the good filler material for the fabrication of

multifunctional composites because of their excellent mechanical property, high electrical and thermal conductivity. Extensive efforts have been made to prepare the nanocomposite of carbon materials and polyaniline for potential applications in many fields. Polyaniline was successfully assembled with poly-(aminobenzenesulfonic acid)-modified single-walled carbon nanotubes through the simple layer-by-layer method and showed a high electrocatalytic ability toward the oxidation of reduced β -nicotinamide adenine dinucleotide at a lower potential.⁶ A nanocomposite of polyaniline derivative, poly-(anilineboronic acid), with ss-DNA-wrapped single-walled carbon nanotubes was reported to detect nano-molar concentrations of dopamine with high sensitivity.⁷ Composites consisting of functionalized single-walled carbon nanotubes in polyaniline and polystyrene sulfonate-doped polyaniline were compared for the bioelectrocatalyzed oxidation of glucose in the presence of glucose oxidase and it was observed that the charge transport properties of the first composite was faster than the later material without carbon nanotubes.⁸ It is also reported that polyaniline can be used as an actuator material due to its chemical and electrochemical stability both in air and moisture and also can operate at isotonic stresses.⁹ The addition of carbon nanotubes to polyaniline fibers produces significant improvements in their electroactivity that translates to enhanced actuation performance.¹⁰

The use of polyaniline and its derivatives has been reported as a catalyst support for many heterogeneous catalysis reactions where palladium nanoparticles act as an active catalyst species.^{11–18} Metal nanoparticles have been increasingly used in the fields of bio-electrochemical applications owing to their extraordinary electrocatalytic activity. The conductivity characteristic of the composite can be greatly increased if the nanoparticles are combined with polymer.³ A nanocomposite with a core-shell structure containing polystyrene, polyaniline and gold nanoparticles showed high catalytic activity for the enzymatic oxidation of glucose.¹⁹ Composite of polyaniline and mercaptosuccinic-acid-capped gold nanoparticles shows electrocatalytic activity towards oxidation of NADH (reduced form of Nicotinamide Adenine Dinucleotide) and also be utilized to detect DNA hybridization by an electrochemical method.²⁰ Composite materials consisting of polyaniline-co-poly (4-styrene sulfonate) and polyaniline-gold nanoparticles capped with 2-mercaptoethane sulfonic acid were used as electrocatalyst for the enzymatic oxidation of glucose and the amperometric experiments reveal that the charge transport in the polyaniline-gold system is 25-fold higher as compared to the polyaniline-styrene system.²¹ A composite hollow sphere of polyaniline-gold with high electrocatalytic activity was

successfully applied to construct a sensor for the recognition of dopamine, an important neurotransmitter in mammalian central nervous system.²²

Composite architecture fabricated with silver nanoparticles as one of the component shows some interesting properties as an electrochemical sensor for the detection hydrogen peroxide.^{23, 24}

Again, enzyme-free electrochemical method for the detection of hydrogen peroxide has been reported using copper-oxide system.²⁵ Among the various analytical methods,²⁶⁻²⁸ electrochemical technique provides the simple, economic and sensitive detection for hydrogen peroxide. Enzymatic electrochemical sensor possesses good sensitivity and selectivity²⁹ but there are some disadvantages of the enzyme-modified electrodes, such as, instability, high cost of enzymes, complicated immobilization technique, and critical operating procedure.³⁰ Therefore, considerable attention has been paid to develop the nonenzymatic electrochemical detection method to solve these problems that seems to be an extremely attractive alternative technique free from the above mentioned drawbacks. Detection of hydrogen peroxide is an important practice in food and pharmaceutical industry and also in clinical, environmental and biological research sector. An electrochemical method with an enzyme free system therefore attracts enormous attention towards a rapid and sensitive detection of hydrogen peroxide.

With the progress of nanoscience and nanotechnology based research, metal nanoparticles have been widely used to fabricate nonenzymatic sensors due to their unique properties of biocompatibility, improved electrical property and low toxicity. As a typical nanomaterial, silver nanoparticle exhibits excellent physicochemical properties and shows good catalytic activity toward the fabrication of hydrogen peroxide sensor.

In this present communication, we report an *in-situ* synthesis technique for the preparation of 'silver-polymer' supramolecular composite material by applying an "*in-situ* polymerization and composite formation" (IPCF) type of reaction^{1, 31, 32} using silver nitrate as an oxidizing agent for polymerizing 4-(thiophen-3yl)-aniline. During the polymerization process, each step is associated with a release of electrons and that reduces the Ag(I) ion to form Ag(0). The Ag(0), silver nanoparticle, which acts as the active site of the catalyst, stabilized in the poly-[4-(thiophen-3yl)-aniline], *p*T3A, with the formation of metal-polymer composite, Ag(0)-*p*T3A, and has been used as an electrocatalyst for the nonenzymatic detection of hydrogen peroxide.

2. Experimental:

2.1. Materials: All the chemicals and the solvents used for this experiment were of analytical purity and used without further purification. Ultra-pure water (specific resistivity $>17 \text{ M}\Omega \text{ cm}$) was used in this experiment wherever required.

2.2. Procedure:

Synthesis of Ag(0)-pT3A and pT3A: In a typical reaction, silver nitrate ($1.0 \times 10^{-3} \text{ mol dm}^{-3}$, 5.0 mL) was added to the 10 mL of 4-(thiophen-3yl)-aniline, T3A, in methanol, with the concentration of $0.5 \times 10^{-2} \text{ mol dm}^{-3}$ under continuous stirring conditions. After the complete addition, the solution was allowed to stand at rest for 30 min and subsequently TEM specimens were prepared by pipetting 2 μL of the deposited material onto lacey carbon coated copper grids. A small portion of the product was used for optical characterization, the remaining fraction being dried under vacuum for different analytical testing and also for catalytic activity studies. In a separate reaction, 5.0 mL of ammonium persulphate ($1.0 \times 10^{-3} \text{ mol dm}^{-3}$) was added to the 10 mL of 4-(thiophen-3yl)-aniline ($0.5 \times 10^{-2} \text{ mol dm}^{-3}$) under the above mentioned reaction condition. The solid product obtained was used as control material for the rest of the reaction.

2.3. Material characterization: Fourier transform infrared spectroscopy (FTIR) spectra were collected utilizing a Shimadzu IRAffinity-1 with a spectral resolution of 0.5 cm^{-1} . The UV-vis spectra were measured using a Shimadzu UV-1800 spectrophotometer with a quartz cuvette. To measure the fluorescence sensitivity of the material a spectrofluorophotometer (RF-5301PC, Shimadzu), attached with a light source of 150W Xenon lamp, was used for this study. Transmission electron microscopy (TEM) studies of the nanocomposite were carried out at 197 kV using a Philips CM200 TEM equipped with a LaB_6 source. An energy-dispersive X-ray analyser (EDX) attached to the TEM was used to determine the chemical composition of the samples. The X-ray diffraction (XRD) patterns were recorded on a Shimadzu XD-3A X-ray diffractometer operating at 20 kV using $\text{Cu-K}\alpha$ radiation ($k = 0.1542 \text{ nm}$). The measurements were performed over a diffraction angle range of $2\theta = 10^\circ$ to 80° . X-ray photoelectron spectra (XPS) were collected in a UHV chamber attached to a Physical Electronics 560 ESCA/SAM instrument. Electrochemical measurements were carried out with a, Bio-Logic, SP-200, potentiostat connected to a data controller. A three-electrode system was used in the experiment

with a glassy carbon electrode (GCE) as the working electrode. Ag/AgCl electrode (saturated KCl) and a Pt electrode were used as the reference and counter electrodes respectively.

2.4. Catalytic hydrogenation study: For this experiment, the probe 4-nitrophenolate (4NP) was made by adding sodium hydroxide to the water solution of 4-nitrophenol with a final concentration of 10^{-4} mol dm $^{-3}$. The catalytic hydrogenation study of 4NP was performed in presence of sodium borohydride (10^{-3} mol dm $^{-3}$) as a reducing agent using the silver-polymer composite, Ag(0)-*p*T3A, as a catalyst and the progress of the reaction was monitored using a spectrophotometer. A control experiment was also done to check the activity of the polymer (*p*T3A) as a catalyst.

2.5. Electrocatalytic study: Both the polymer, *p*T3A, and the silver-polymer composite, Ag(0)-*p*T3A, were deposited on the working electrode using a 'drop and dry' method. After each run, the electrode was washed and an identical amount of new catalyst was applied as a coating to the electrode for the next study for the electrocatalytic detection of hydrogen peroxide.

3. Result and discussion:

Nanotechnology has an extremely broad range of potential applications in the fields of electronics, optics, biology and medicine and therefore it requires the contribution from multidisciplinary teams of physicists, chemists, materials scientists, engineers, molecular biologists to work together on the synthesis and processing of nanomaterials, understanding the physical properties and design and fabrication of devices for various applications. Characterization is an important step and should be performed at the beginning before find out the potential application of the particular material.

In this current study, we have chosen 4-(thiophen-3yl)-aniline, a derivative of aniline, and a metal salt, silver nitrate, as the starting materials for the synthesis of metal-polymer supramolecular composite. A wide variety of methods have been applied to the preparation of conjugated polyaniline or substituted polyaniline-type of compounds by the oxidative polymerization of their monomer.³³ According to the most widely accepted mechanism, the first step during the polymerization of aniline or substituted aniline involves the formation of a radical cation accompanied by the release of an electron. This step is the initiation process of the polymerization reaction. Here, silver nitrate was used as an oxidizing agent and during

polymerization the released electrons reduced the silver ions to form silver atoms. The coalescence of these atoms ultimately forms nanoparticles, which are encapsulated and stabilized by the polymer and the method is known as ‘*in-situ* polymerization and composite formation (IPCF)’ in which both the polymer and the nanoparticles are produced simultaneously that facilitate an intimate contact between both the particles and the polymer through functionalization.^{1, 34–39}

The absorption spectrum (Figure 1A) for both Ag(0)-*p*T3A (a) and *p*T3A (b) show absorption peaks around 320 nm which are due to the π - π^* transition of the benzenoid rings. The magnified spectra are also shown within *in-set*. A shoulder-like appearance is observed for *p*T3A within the range of 400–500 nm due to the polaron–bipolaron transition. An identical appearance has also been observed for Ag(0)-*p*T3A within the range of between 360–500 nm with a peak value at 420 nm resulted from the combined effect of surface plasmon absorption band for silver nanoparticle and the polaron–bipolaron transition. A low intensity absorption band between 500–600 nm has been observed for Ag(0)-*p*T3A, spectrum (a), and that corresponds to the benzenoid-to-quinoid excitonic transition. The presence of quinoid unit in the metal-polymer composite has been confirmed using a Fourier transform infrared spectroscopy technique, where the vibrational signature at 1650 cm^{-1} indicates the presence of N=Q=N, where Q represents a quinoid ring structure. The bands at 1110 and 1013 cm^{-1} are due to the aromatic C–H *in-plane* bending modes. A doublet band with the peak positions at 1402 and 1450 cm^{-1} can be assigned to the ν_3 mode of thiophene⁴⁰ present in the polymer structure. The ν_3 mode is a ring vibration that consists primarily of the symmetric stretching of the C=C bonds of thiophene.^{41, 42} A broad band observed at 3400 cm^{-1} corresponds to the –OH stretching vibration from the solvent. Two bands at 2833 and 2940 cm^{-1} are responsible for C–H stretching vibration.

Figure 2A displays a transmission electron microscope (TEM) image of the metal-polymer supramolecular composite. This image was taken from a less dense area and shows the high density distribution of dark spots in the polymer. A typical EDX spectrum (Figure 2C) obtained from the electron beam being focused onto a dark spot in the polymer confirms that these spots are silver particles. The TEM image clearly indicates that the 7–12 nm diameter nanoparticles are well dispersed within the polymer matrix (Figure 2A). The silver particles were found to be homogeneously distributed within and throughout the polymer matrix. The higher magnification TEM image of a single silver particle exhibiting the lattice fringes of spacing 0.24 nm (Figure

2B). We have also have performed the X-ray photoelectron spectroscopy (XPS) measurement to identify the chemical state of the polymer stabilized silver nanoparticles at the Ag 3d core levels. In the high-resolution Ag 3d XPS spectrum (Figure 3D), two peaks located at the binding energies of 366.87 and 373.12 eV were observed, which is consistent with the emission of 3d photoelectrons from Ag(0) and thereby confirming the successful formation of metallic silver nanoparticles⁴³ in the polymer matrix. The metallic nano-crystals were found to be highly face selective as can be seen from the XRD pattern of Ag(0)-*p*T3A in Figure 3E. The strong Bragg reflection from the (111) lattice planes indicates the highly oriented crystalline character of the nanoparticles. Three weak Bragg peaks from the (200), (220) and (311) planes also indicate the anisotropic nature of the particles.

Photoluminescence spectra for the polymer and silver-polymer were measured in the range of 300 – 850 nm and shown in figure 3A. The wavelength of excitation for the samples was chosen 300 nm as it fall within the range of π - π^* absorption envelop of the benzenoid units centered at 320 nm. In the current experiment, the emission peak was observed for both the samples at about 370 nm and it is also evident from the figure that the intensity of the spectra for Ag(0)-*p*T3A is higher than that of the pure polymer. It has been well documented that benzenoid unit present in the polyaniline backbone demonstrate the fluorescence property. The photoluminescence property of polyaniline is caused by the benzenoid unit (amine group) and it is quenched when such a group is adjacent to the quinoid unit (imine group) or converted to a quinoid unit.⁴⁴ So, in both samples benzenoid groups are predominantly present than the quinoid units. The presence of both amine group (electron donating group) and silver particle (an electron conducting species) enhances the electron mobility in the Ag(0)-*p*T3A composite, which in turn favours the formation of singlet excitons. Exciton is an elementary excitation state of matter that can transport energy without transporting electric charge. The singlet exciton states decay radiatively to the ground state resulting in enhanced photoluminescence.⁴⁵ A broader spectrum appeared for Ag(0)-*p*T3A composite and may be attributed due to the formation of more density of states in the presence of silver nanoparticles. A low intensity peak at the higher wave length region (in the range of 700-800 nm, the magnified zone, shown by an arrow) has been observed and a similar event, as above, can be predicted for both the samples.

The photoluminescence spectra of Ag(0)-*p*T3A in various solvents, for both lower (350-450 nm) and higher (675-800 nm) wavelength region, are shown in figure 3B. When toluene was used as

a solvent for the chromophore, the peak position of the emission spectra (f) was found at 363 nm, whereas for the high polarity solvents, like DMF, the peak position of the spectra (e) has been shifted to 370 nm. A similar kind of behaviour has been noticed at the higher wavelength region as well but with a lower intensity. The spectral shift of the chromophore is strongly dependent on the polarity of the solvent. Changing the solvents with different polarities lead to different stabilization of the ground and excited states of the chromophore and consequently an alteration in the energy gap between these electronic states, results the variations in the position, intensity and shape of the spectra.

3.1. Catalytic property of Ag (0)-*p*T3A:

Catalysis by metal nanoparticles is certainly among the most intensely studied problems in nanoscience and nanotechnology. The comparative studies for catalytic performance of such particles are not always possible due to their non-identical support system, different solvent and synthesis conditions. In the current manuscript, the catalytic property of silver nanoparticles, stabilized within the polymer matrix, has been tested by following the reduction process of 4-nitrophenolate ion (*4-NP*), a model reaction generally used to check the catalytic activity of metal nanoparticles. For more information, the reader is referred to a tutorial review by Ballauff and co-workers.⁴⁶

To explore the catalytic property of synthesized compounds (*p*T3A and Ag(0)-*p*T3A), two sets of experiments has been performed. The solution of *4-NP* exhibited an absorption peak at 400 nm (Figure 4, *in-set*, spectrum a). Upon the addition of NaBH₄ (20 μL) and *p*T3A, the wavelength value of the spectra remain unchanged but a slight decrease in intensity has been observed (Figure 4, *in-set*, spectrum b). The interesting thing happened when Ag(0)-*p*T3A (amount of Ag present in the composite was 0.06 mg) was added in presence of *4-NP* and NaBH₄ (20 μL). After the addition of silver-polymer composite, the intensity of the absorption peak of *4-NP* has been gradually decreased and the time required for complete quenching of the spectra was 12 min (Figure 4A, the main panel) indicates the catalytic property of the silver nanoparticles in the polymer based composite material. Sodium borohydride is a strong reducing agent but the reduction of *4-NP* in presence of borohydride was not possible due to the kinetically unfavourable condition whether in presence of silver nanoparticles a smooth

reduction of *4-NP* has been observed because the nanoparticles act as a catalyst that breaks the kinetic barrier for the reduction reaction.

Figure 4B show the plot (C_t/C_0) as a function of time for the reduction of *4-NP* in presence of Ag(0)-*pT3A* as catalysts and the quenching of the colour of *4-NP* at the end of the complete reduction (cuvette 1 and 2, are for before and after the reduction, respectively). The rate constant for the reduction was found to be $1.15 \times 10^{-2} \text{ min}^{-1}$.

3.2. Electrocatalytic performance of Ag(0)-*pT3A* for the detection of H_2O_2 :

Inspired by the above results, we have further explored the performance of the silver catalyst for the electrocatalytic detection of hydrogen peroxide, an important biological substance plays a significant role in many fields such as textile, food and paper industry, pharmaceutical industry, medical diagnostics, in a non-enzymatic pathway.

At first we have performed the electrochemical impedance study for the samples, *pT3A* and Ag(0)-*pT3A*, which is a useful technique for probing the features of surface modified electrodes. In the impedance spectra, the semicircle part at high frequency correspond to the electron transfer limited process and a linear part at lower frequency demonstrate the diffusion-limiting step of the electrochemical process. The semicircle diameter equal to the electron transfer resistance at the electrode surface. Figure 5 shows the electrochemical impedance spectra for the Ag(0)-*pT3A* (spectrum a) and *pT3A* (spectrum b). In the figure, a straight line observed at lower frequencies for both samples, which is the characteristic of a diffusion-limiting step of the electrochemical process. For the sample *pT3A*, the electron transfer resistance was significantly expanded which indicated the polymer performs as a kinetic barrier for the electron transfer, whereas, in Ag(0)-*pT3A* the electron transfer resistance was decreased due to the presence of silver nanoparticle that participate a key role similarly to an electron-conducting tunnel and therefore promoting an efficient charge transfer mechanism.

In this current work, we have compared the affinity and sensitivity of *pT3A* and Ag-*pT3A* for the electrochemical detection of hydrogen peroxide using the cyclic voltammetry (CV) technique in milli-Q water, at the scan rate of 0.05 V/s^{-1} (Figure 6). Inset figure A(i) represents the cyclic voltammograms for bare GCE in the absence (curve 'a') and presence (curve 'b') of analyte (H_2O_2). An enhanced current signal has been observed when H_2O_2 (0.2 mM) was used as an analyte for bare unmodified electrode. When electrode was modified with *pT3A* an enhancement of the anodic current, compared to the bare one, for both in the absence (curve 'a') and presence

(curve 'b') of analyte, inset figure A(ii), has been observed indicating the electro-oxidation of the polymer. A slight enhancement of the anodic current value (curve 'b', continuous line) has also been observed in presence of H_2O_2 for *p*T3A modified GCE. Figure 6A, the main panel, shows the voltammograms for Ag(0)-*p*T3A modified electrode on the recognition of hydrogen peroxide. In absence of peroxide, the anodic current signal was improved than the bare, figure A(i), and *p*T3A, figure A(ii), modified electrode indicates the effect of oxidation for both the polymer and zerovalent silver species. The Ag(0)-*p*T3A modified GC electrode exhibited enhanced electrocatalytic oxidation in presence of peroxide (0.2 mM) with the anodic peak current value $10.40 \mu\text{A}$ at the applied potential value 0.600 V (Figure 6A, curve b). These results indicated that Ag(0)-*p*T3A exhibited excellent electrocatalytic activity toward the oxidation of peroxide, and such enhanced activity is due to the introduction of metallic silver, which promotes the electron transfer process.

From the cyclic voltammetry study we have the indication about the electrocatalytic performance of the composite material for the detection of peroxide. The performance of the same catalyst was further studied by differential pulse voltammetry (DPV) technique using various amounts of peroxide concentration. Figure 6B shows the differential pulse voltammograms with the gradual increase of current intensity (curves: b-g) due to the addition of peroxide with different concentration. The voltammogram (a) is for the zero concentration of peroxide. The above technique was also supported by the square wave voltammetry (SWV) technique (Figure 6C), again, using the various peroxide concentrations at the frequency of 20 Hz. With increasing the concentration of the peroxide a steady increase of current intensity has been observed. In the absence of peroxide, no characteristic peak has been observed in the referred potential zone (Figure 6C, curve a). For the present study, it is also important to mention that the SWV technique is more sensitive than DPV technique, for instance, using the concentration of peroxide 1.5 mM the anodic current reach about $1.2 \mu\text{A}$, whereas, for the same concentration of peroxide, the SWV technique showed the current value above $1.5 \mu\text{A}$. The oxidation peak for hydrogen peroxide appeared at different potentials for two above mentioned techniques, for DPV technique the peak appeared at 0.5V whether for SWV technique the peak appeared at 0.3V. For an amperometric technique (differential pulsed), a steady increase in current response has been obtained with the addition of peroxide, to the electrolyte (milli-Q water), from 0.1 to 2.0 mM

(Figure 7, *main panel*), with a regression coefficient and sensitivity value of 0.9996 and 2.131 $\mu\text{A mM}^{-1} \text{cm}^{-2}$, respectively, at 0.4 V (Figure 7, *in-set A*).

The above results indicate that the Ag(0)-*p*T3A composite could be a potential material for the fabrication of a nonenzymatic hydrogen peroxide sensor. We have also performed the “effect of pH” study of the catalyst and found that the silver-polymer composite is tolerant under acidic and basic conditions within a pH range from 2 to 12, respectively, for the detection of peroxide. Selectivity is an important parameter for the fabrication of non-enzymatic sensors. In this study, some potential interfering species (uric acid, glucose, and histamine) have been investigated under a working potential of 0.4 V and the results are shown in figure 7 (*in-set B*). Peroxide solution (0.1 mM) was first injected into the electrolyte (milli-Q water) followed by the addition of interfering species, uric acid, glucose and histamine, (0.1 mM), sequentially and the Ag(0)-*p*T3A modified electrode exhibited good passiveness towards electroactive interference species.

4. Conclusion:

This study describes the method of synthesis polymer stabilized silver nanoparticles in a single step ‘*in-situ* polymerization and composite formation (IPCF)’ protocol. The metal particles formed are in the range of 7-12 nm and stabilized within the polymer matrix. The composite material shows different optical properties, such as, absorption, transmission and luminescence. The silver nanoparticle containing polymer based hybrid material has been successfully utilized as an efficient catalyst for the reduction of aromatic nitro compound, where metal nanoparticle act as the active catalytic centre responsible for the reduction reaction. The active silver was also used as catalyst species for the enzyme-less electrochemical hydrogen peroxide detection. The results showed that the silver-polymer composite was very sensitive for different electrochemical techniques for the efficient recognition of peroxide. In addition, excellent analytical feature, moderately high sensitivity with reproducibility and low detection limits of the catalyst could further make the present material as a promising candidate for the construction of nonenzymatic electrochemical sensors for wide range of analytes of interest.

Acknowledgments:

The authors (M.C, S.S and K.M.) acknowledge financial support from the Research Committee and the Faculty of Science of the University of Johannesburg. M.C. also acknowledges financial

support from the National Research Foundation, South Africa. S.S. further acknowledges financial support from the Global Excellence and Stature fellowship from the University of Johannesburg.

References:

1. K. Mallick, M. Witcomb, R. Erasmus, A. Strydom, *J. Appl. Phys.*, 2009, **106**, 074303.
2. K. Mallick, M. Witcomb, M. Scurrrell, *J. Phys.: Condens. Matter*, 2007, **19**, 196225.
3. K. Mallick, M. Witcomb, M. Scurrrell, A. Strydom, *J. Phys. D: Appl. Phys.*, 2009, **42**, 095409.
4. M. Riskin, B. Basnar, Y. Huang, I. Willner, *Adv. Mater.*, 2007, **19**, 2691-2695.
5. A. A. Syed, M. K. Dinesan, *Talanta*, 1991, **38**, 815-837.
6. J. Liu, S. Tian, W. Knoll, *Langmuir*, 2005, **21**, 5596-5599.
7. Y. Ma, S. R. Ali, A. S. Dodoo, H. He, *J. Phys. Chem. B*, 2006, **110**, 16359-16365.
8. E. Granot, B. Basnar, Z. Cheglakov, E. Katz, I. Willner, *Electroanalysis*, 2006, **18**, 26-34.
9. R. H. Baughman, *Synth. Met.*, 1996, **78**, 339-353.
10. G. M. Spinks, V. Mottaghitalab, M. Bahrami-Samani, P. G. Whitten, G. G. Wallace, *Adv. Mater.*, 2006, **18**, 637-640.
11. M. Choudhary, R. Islam, M. Witcomb, M. Phali, K. Mallick, *Appl. Organometal. Chem.*, 2013, **27**, 523-528.
12. M. Choudhary, R. Islam, M. Witcomb, K. Mallick, *Dalton Trans.*, 2014, **43**, 6396-6405.
13. S. Mahato, R. Islam, C. Acharya, M. Witcomb, K. Mallick, *ChemCatChem*, 2014, **6**, 1419-1426.
14. R. Islam, S. Mahato, S. Shukla, M. Witcomb, K. Mallick, *ChemCatChem*, 2013, **5**, 2453-2461.
15. R. Islam, M. Witcomb, M. Scurrrell, W. Van Otterlo, E. van der Lingen, K. Mallick, *Synthetic Commun.*, 2011, **41**, 3561-3572.
16. R. Islam, M. Witcomb, M. Scurrrell, E. van der Lingen, W. Van Otterlo, K. Mallick, *Catal. Sci. Tech.*, 2011, **1**, 308-315.
17. R. Islam, M. Witcomb, M. Scurrrell, E. van der Lingen, M. Scurrrell, W. Van Otterlo, K. Mallick, *J. Organomet. Chem.*, 2011, **696**, 2206-2210.
18. R. Islam, M. Witcomb, M. Scurrrell, W. Van Otterlo, K. Mallick, *Catal. Commun.*, 2010, **12**, 116-121.
19. Y. Liu, X. Feng, J. Shen, J. J. Zhu, W. Hou, *J. Phys. Chem. B*, 2008, **112**, 9237-9242
20. S. Tian, J. Liu, T. Zhu, W. Knoll, *Chem. Mater.*, 2004, **16**, 4103-4108.
21. E. Granot, E. Katz, B. Basnar, I. Willner, *Chem. Mater.*, 2005, **17**, 4600-4609.

22. X. Feng, C. Mao, G. Yang, W. Hou, J. J. Zhu, *Langmuir*, 2006, **22**, 4384-4389.
23. S. Zhang, Q. Sheng, J. Zheng, *RSC Adv.*, 2015, **5**, 26878-26885.
24. K. E. Hnida, R. P. Socha, G. D. Sulka, *J. Phys. Chem. C*, 2013, **117**, 19382-19392.
25. J. Hennemann, C. Kohl, S. Reisert, P. Kirchner, M. J. Schöning, *Phys. Status Solidi (A)*, 2013, **2110**, 859-863.
26. E. Zapp, V. Nascimento, D. Dambrowski, A. L. Braga, I. C. Vieira, *Sens. Actuators B*, 2013, **176**, 782-788.
27. L. J. Zhang, Y. C. Chen, Z. M. Zhang, *Sens Actuators B*, 2014, **193**, 752-758.
28. M. M. Vdovenko, A. S. Demiyanova, K. E. Kopylov, I. Y. Sakharov, *Talanta*, 2014, **125**, 361-365.
29. Z. Matharu, J. Enomoto, A. Revzin, *Anal. Chem*, 2013, **85**, 932-939
30. M. Choudhary, S. Shukla, A. Taher, S. Siwal, K. Mallick, *ACS Sustainable Chem. Eng*, 2014, **2**, 2852-2858
31. K. Mallick, M. Witcomb, A. Dinsmore, M. Scurrrell, *Langmuir*, 2005, **21**, 7964-7967.
32. K. Mallick, M. Witcomb, A. Dinsmore, M. Scurrrell, *Macromol. Rapid Commun*, 2005, **26**, 232-235.
33. I. Sapurina, M. Shishov, 'New Polymers for Special Applications', Ed: A. De Souza Gomes, ISBN 978-953-51-0744-6, Publisher: InTech.
34. K. Mallick, M. Witcomb, M. Scurrrell, *Euro. Phys. J. E*, 2006, **20**, 347-353.
35. K. Mallick., M. Witcomb, M. Scurrrell, *J. Mater. Sci*, 2006, **41**, 6189-6192.
36. K. Mallick, M. Witcomb, M. Scurrrell, *Euro. Phys. J. E*, 2006, **19**, 149-154.
37. K. Mallick., M. Witcomb, M. Scurrrell, *Euro. Poly. J*, 2006, **42**, 670-675.
38. K. Mallick., M. Witcomb, M. Scurrrell, *Mater. Sci. Eng. B*, 2005, **123**, 181-186.
39. K. Mallick, M. Witcomb, M. Scurrrell, A. Strydom, *Gold Bull*, 2008, **41**, 246-249
40. A. A. El-Azhary, R. H. Hilal, *Spectrochim. Acta*, 1997, **53**, 1365-1373.
41. D. W. J. Scott, *J. Mol. Spectroscopy*, 1969, **31**, 451-463.
42. Z. Wu, C. Li, Z. Wei, P. Ying, Q. Xin, *J. Phys. Chem. B*, 2002, **106**, 979-987.
43. S. Gao, D. Chen, Q. Li, J. Ye, H. Jiang, C. Amatore, X. Wang, *Sci. Rep.*, 2014, **4**, 4384.
44. J. Y. Shimano, *Synth. Metals*, 2001, **123**, 251-262.

45. D. L. Wise, G. E. Wnek, D. Trantolo, T. M. Cooper, J. D. Gresser, Photonic polymer systems-Fundamentals, methods and applications, ISBN 9780824701529 (New York: Marcel Dekker, Inc. 1998)
46. P. Hervés, M. Pérez-Lorenzo, L. M. Liz-Marzán, J. Dzubiella, Y. Lubc, M. Ballauff, *Chem. Soc. Rev.*, 2012, **41**, 5577-5587.

Figure caption:**Figure: 1**

(A) The UV-vis spectra for both *p*T3A (spectrum 'b') and Ag(0)-*p*T3A (spectrum 'a') show absorption peaks around 320 nm which are due to the $\pi-\pi^*$ transition of the benzenoid rings (inset: the magnified peak positions). (B) The FTIR spectrum show different vibrational signature of the Ag(0)-*p*T3A.

Figure: 2

(A) TEM image of the metal-polymer composite material where the dark spots are the silver nanoparticles, within the size range of 7–12 nm, stabilized in the polymer matrix. (B) The higher magnification TEM image of the silver nanoparticle exhibiting the lattice fringes. (C) EDX analysis of the composite, where the silver peak from the silver particles, and the Cu and S peaks originated from the TEM support grid and the thiophene moiety of the polymer, respectively. (D) The high resolution XPS spectrum of the silver-polymer composite has two peaks with the binding energy values 373.12 and 366.87 eV are assigned for the Ag 3d_{5/2} and Ag 3d_{3/2} orbits respectively, indicate the formation of metallic silver. (E) The XRD pattern indicates the highly face selective silver nanoparticles with a strong Bragg reflection from the (111) lattice planes.

Figure: 3

(A) Photoluminescence spectra of *p*T3A (spectra 'a') and Ag(0)-*p*T3A (spectra 'b') in methanol as a solvent (0.5×10^{-4} M), *in-set* is the magnified spectra from the marked area. (B) Comparative photoluminescence spectra of Ag(0)-*p*T3A in various solvents (0.5×10^{-4} M).

Figure: 4

(A), In-set, the spectrum (a) with the absorption maxima at 400 nm for 4-*NP* and the spectrum (b), after the addition of NaBH₄ and *p*T3A and no further decrease in intensity has been observed of the spectra for next 5h. In the main panel, the spectrum (a) with the absorption maxima at 400 nm for 4-*NP* and after the addition of NaBH₄ and Ag(0)-*p*T3A, the gradual decrease of intensity of the peak has been observed. (B), shows the plot (C_t/C_0) as a function of time for the reduction of 4-*NP* in the presence of Ag(0)-*p*T3A as catalysts and the quenching of the colour of 4-*NP* at

the end of the complete reduction (cuvette 1 and 2, are for before and after reduction, respectively).

Figure: 5

Impedance spectra of Ag(0)-*p*T3A (a) and *p*T3A (b) modified glassy carbon electrode within the frequency range from 10^5 Hz to 1.0 Hz, in 5.0 mM hexacyanoferrate (III) with 0.3M KCl.

Figure: 6

(A) In the main panel, cyclic voltammograms (CV) at Ag(0)-*p*T3A modified GCE in the absence (curve 'a'), and presence (curve 'b') of 0.2 mM H₂O₂. In-set figure A(i): CV for bare GCE in the absence (curve 'a') and presence (curve 'b') of 0.2 mM H₂O₂; in-set figure A(ii): CV for *p*T3A modified GCE in the absence (curve 'a') and presence (curve 'b') of 0.2 mM H₂O₂, in milli-Q water, pH 7.0 at scan rate of 0.05 V/s⁻¹. (B) Differential pulse voltammograms for Ag(0)-*p*T3A modified GCE with the increasing concentration of H₂O₂, (a-g), [0, 0.2, 0.5, 0.75, 1.0, 1.2, 1.5] mM, respectively, at the pulse width of 20 ms, scan rate 0.05 V/s⁻¹ in milli-Q water. (C) Square wave voltammograms for Ag(0)-*p*T3A modified GCE with the increasing concentration of H₂O₂, (a-j), [0, 0.2, 0.5, 0.75, 1.0, 1.25, 1.50, 2.0, 2.5 and 3.0] mM, respectively, at the frequency of 20 Hz, in milli-Q water.

Figure: 7

In the main panel, typical amperometric response as a function of time, for Ag(0)-PT3A modified GCE after successive addition of 0.01M H₂O₂ on every 50 sec in milli-Q water using the applied potential 0.4V. In-set (A), calibration curve of H₂O₂, current versus peroxide concentration and in-set (B), interfering effect of uric acid (UA), glucose (Glu) and Histamine (HA), 0.1 mM, on the response of the Ag(0)-*p*T3A modified GCE at the applied potential of 0.4V, in water.

Figure: 1

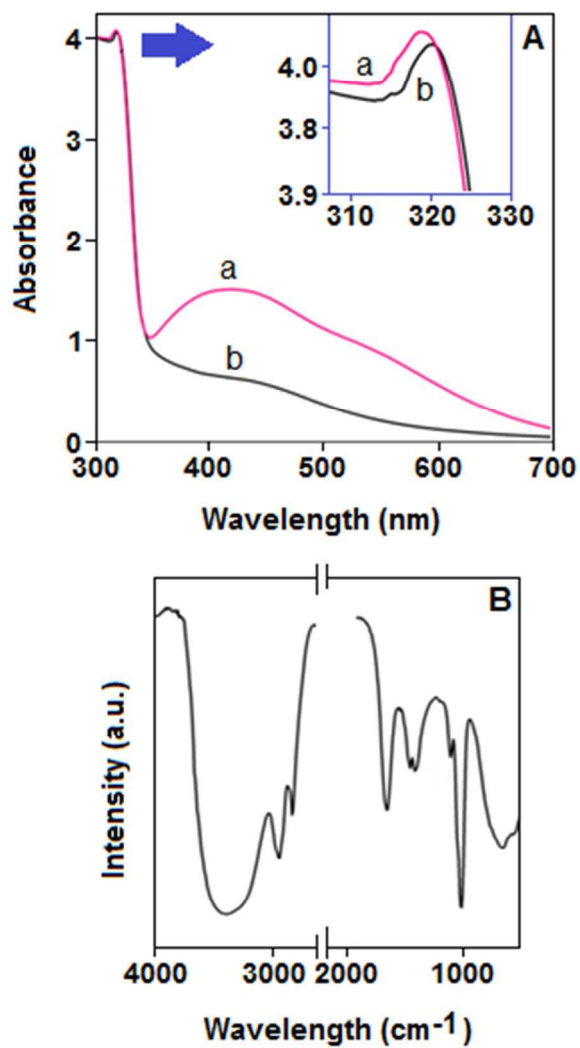


Figure: 2

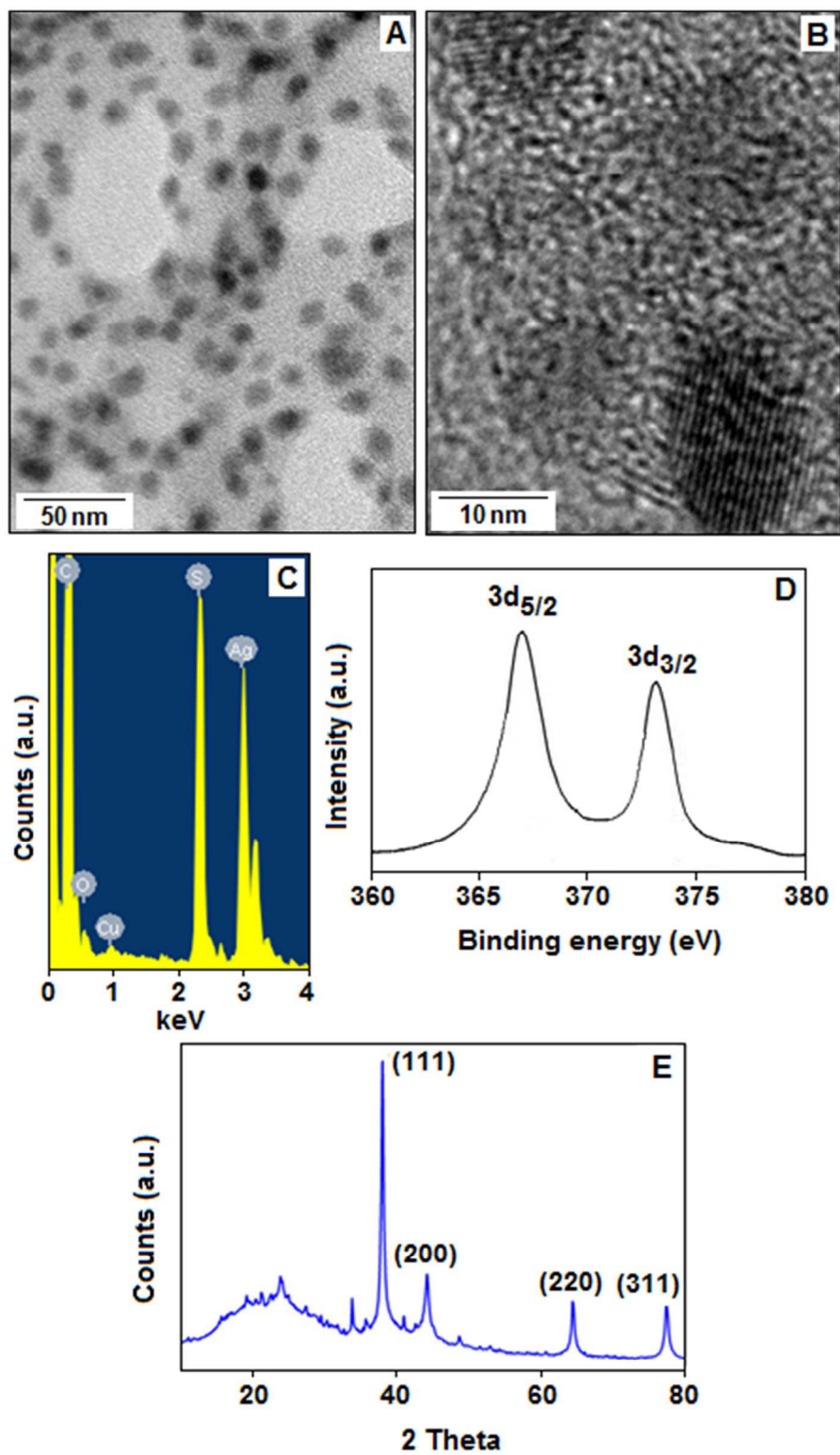


Figure: 3

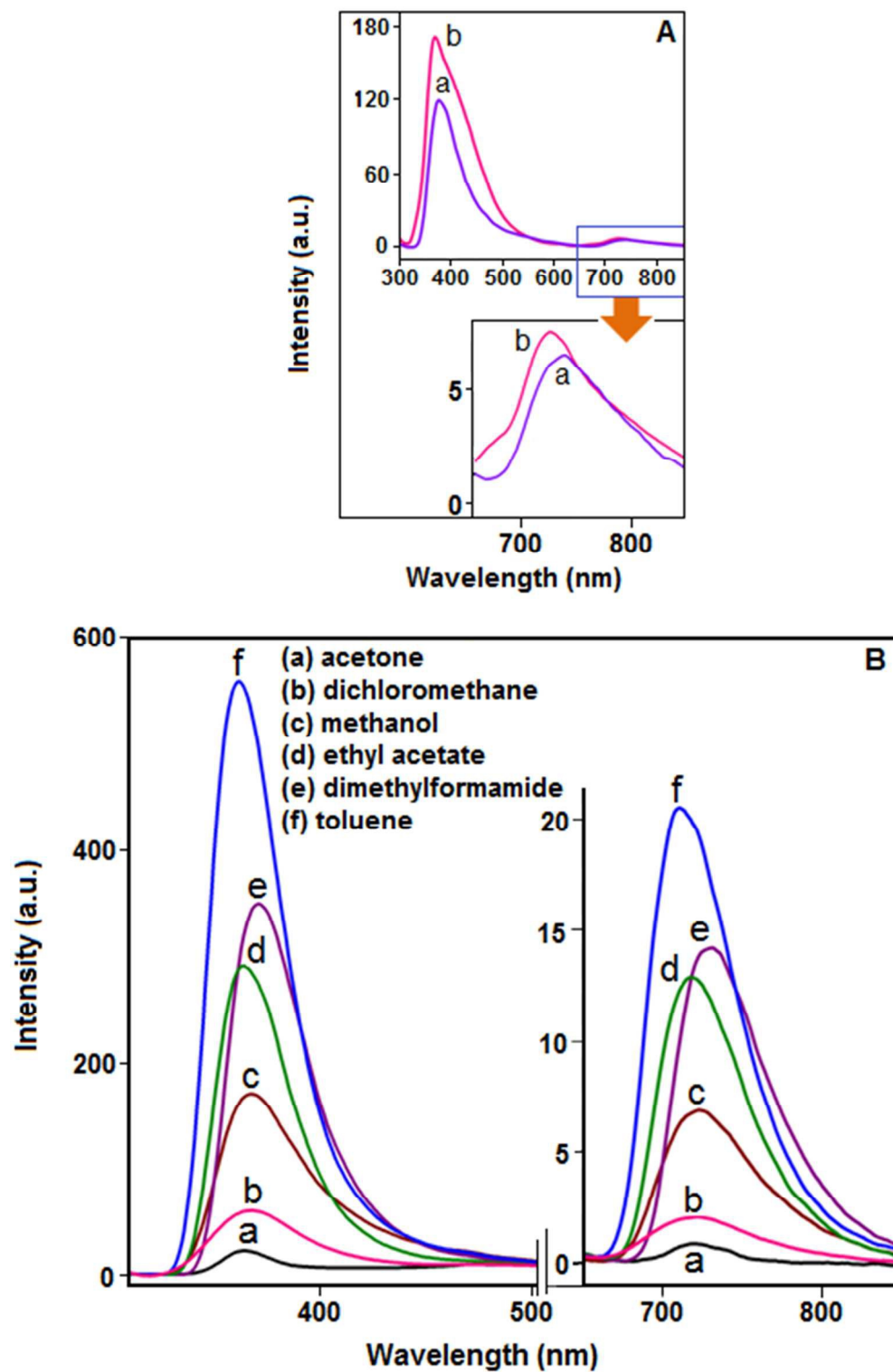


Figure: 4

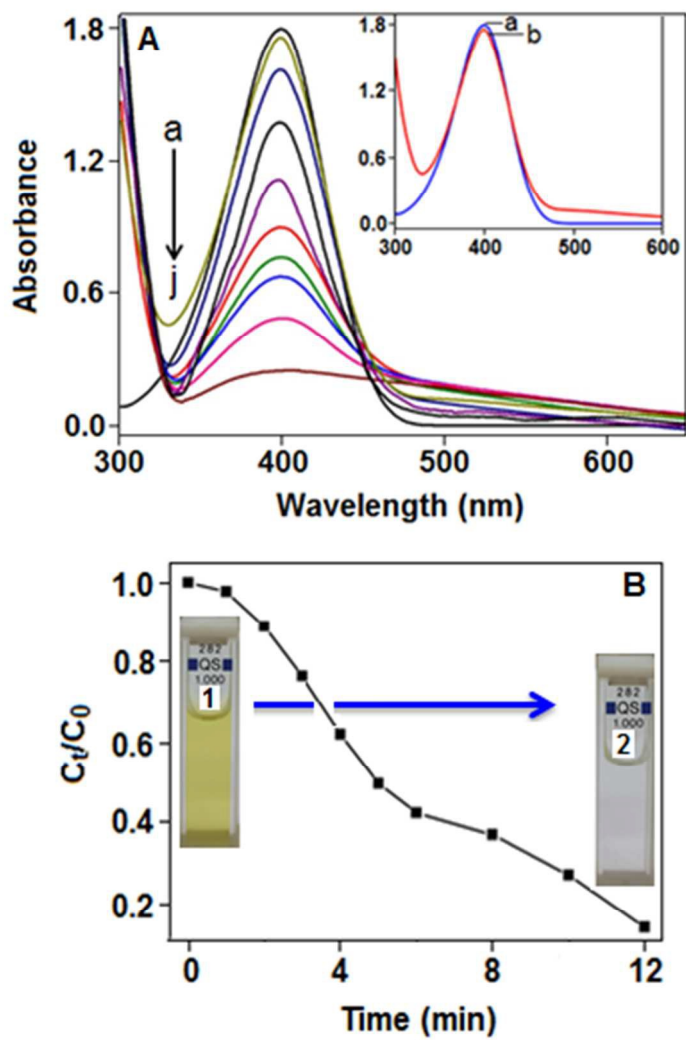


Figure: 5

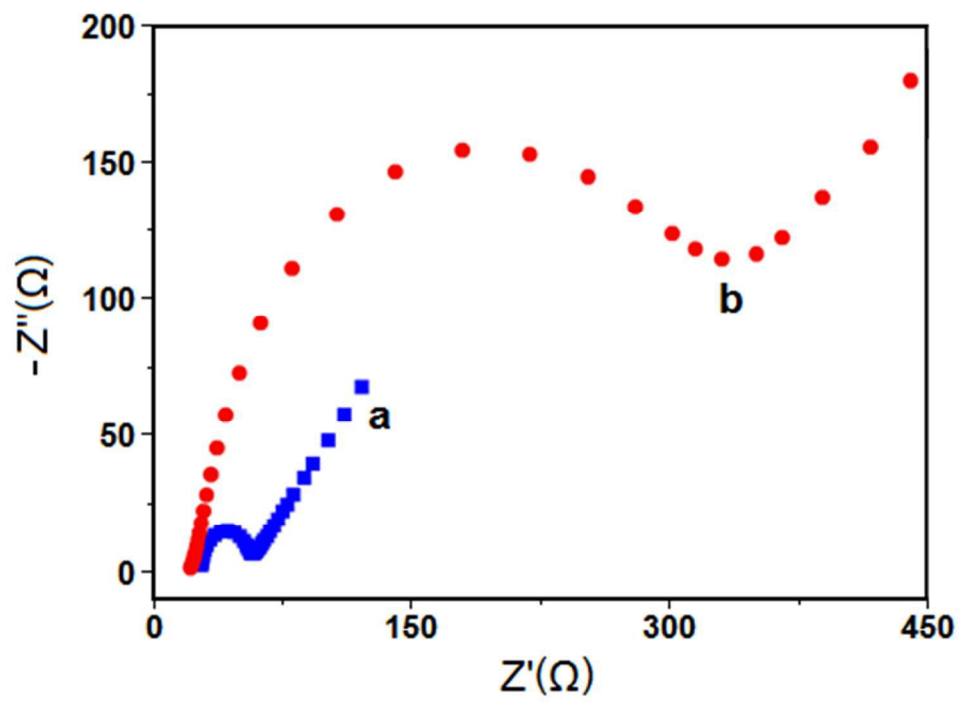


Figure: 6

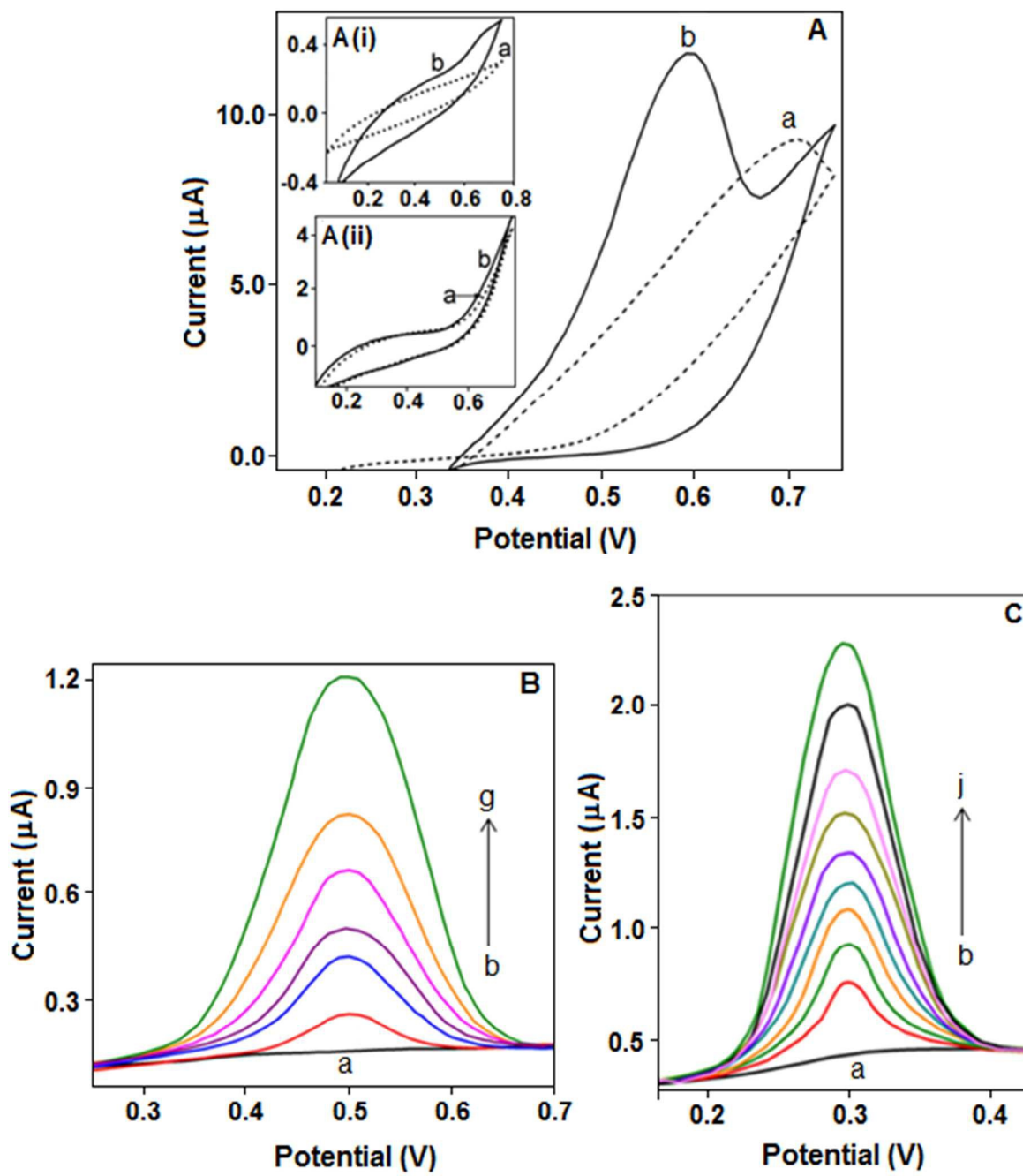


Figure: 7

